

Crossover of Superconductivity across the end point of antiferromagnetic phase in $\text{FeSe}_{1-x}\text{S}_x$ under pressure

Kiyotaka Miyoshi,^{1,2} Hironobu Nakatani,¹ Yumi Yamamoto,¹
Takumi Maeda,¹ Daichi Izuhara,¹ and Ikumi Matsushima,¹

¹*Department of Physics and Material Science, Shimane University, Matsue 690-8504, Japan and*

²*Next Generation TATARA Co-Creation Center, Shimane University, Matsue 690-8504, Japan*

(Dated: May 8, 2025)

Temperature-pressure (T - P) phase diagrams of $\text{FeSe}_{1-x}\text{S}_x$ were investigated by the measurements of dc magnetization (M) and electrical resistivity (ρ) under pressure, using single crystal specimens with $x=0.04, 0.08$ and 0.13 . We observed a crossover of the superconductivity with increasing P near the end point of antiferromagnetic (AFM) phase, where two superconducting phases coexist within a pressure width of $\Delta P \sim 1$ GPa, having different T_c s. These results suggest that the superconducting phases inside and outside the AFM phase have different origins.

I. INTRODUCTION

Since the discovery of superconductivity in $\text{LaFeAsO}_{1-x}\text{F}_x$ [1], a wide variety of iron-based superconductors have been discovered, and unconventional superconductivity realized through the competition or cooperation with the antiferromagnetic (AFM) and nematic phases has been the subject of intensive study, exploring the pairing mechanism[2–4]. Indeed, to establish the phase diagram of various iron-based superconductors is crucial because fluctuations arising from the ordered phase adjacent to the superconducting (SC) phase in the phase diagram are promising candidates for pairing glue. In this context, FeSe is an important subject to explore the T - P phase diagram. Because the nematic phase is decoupled from the AFM phase at ambient pressure unlike other iron-based superconductors, where AFM order is intertwined with nematic correlation, as in AFe_2As_2 ($\text{A}=\text{Sr}, \text{Ba}, \text{Ca}, \text{Eu}$)[5–10], $\text{LaFeAsO}_{1-x}\text{F}_x$ [11], $\text{NaFe}_{1-x}\text{A}_x\text{As}$ ($\text{A}=\text{Co}$ [12, 13], Cu [14]) and SrVO_3FeAs [15, 16], while fourfold enhancement is achieved in its T_c under pressure[17–22]. FeSe has been revealed to have an intriguing T - P phase diagram, where T_c increases rapidly after the nematic phase disappears at ~ 2 GPa[22], accompanying with the emergence of AFM phase above 1.2 GPa[23–27], so that the three phases are competing to each other.

Isovalently substituted $\text{FeSe}_{1-x}\text{S}_x$ is a more desirable material to verify which fluctuation dominates the superconductivity or to search for nematic fluctuation-mediated superconductivity rather than FeSe , since the AFM phase appears at even higher pressure than the pressure of the nematic end point[29], so that both phases are well isolated each other. In $\text{FeSe}_{1-x}\text{S}_x$, whereas the nematic phase is suppressed by the S-substitution toward the nematic quantum critical point at $x \sim 0.17$ [30], T_c is found to be maximized at $x \sim 0.1$ [31], where spin fluctuation is also strongly enhanced[32]. From various measurements and theoretical studies, the SC gap structure is thought to be of superconductivity mediated by spin fluctuation for pure FeSe ($x=0$)[33–35], while sig-

nificant changes in the electronic structure are observed across x_c [36–38], and nematic fluctuation-mediated pairing are suggested for $x > x_c$ [39]. Under pressure, the electronic structure has been investigated by the measurements of nuclear magnetic resonance[40–42] and quantum oscillation[43], suggesting the reconstitution of Fermi surfaces across the nematic end point[44] and the distinction of two superconductivities under presence or absence of nematicity.

For the further understanding of the superconductivity, to study the evolutions of superconductivity not only across the nematic end point but also across the end point of the AFM phase is highly desired. For the purpose, microscopic measurements are necessary to be performed above 3 GPa, although experimental difficulties are faced especially in observing Fermi surface under high pressure due to the restricted experimental approaches at present. To investigate T - P phase diagram of $\text{FeSe}_{1-x}\text{S}_x$, electrical resistivity (ρ) measurements have been performed under pressure up to ~ 8 GPa using a cubic anvil apparatus (CAA) which generates hydrostatic pressure[29], in addition to the detailed $\rho(T)$ measurements below 2 GPa[45]. Through these studies, a notable trend that an isolation between the nematic and AFM phases becomes remarkable in the specimens with higher x has been unveiled, but the detail of the boundary lines of SC and AFM phases remain unclear due to the large pressure intervals of ~ 1 GPa in the measurements[29].

In the present work, we have performed the measurements of dc magnetization and electrical resistivity under pressure up to 6 GPa using single crystal specimens of $\text{FeSe}_{1-x}\text{S}_x$ ($x=0.04, 0.08$ and 0.13) to establish the T - P phase diagram. We report the occurrence of the crossover of the superconductivity across the end point of the AFM phase, where the $M(T)$ curves show a diamagnetic response in two steps, corresponding to the appearance of two distinct SC phases with different T_c s. T - P phase diagrams, where three superconducting phases SC1, SC2 and SC3 appear, are proposed.

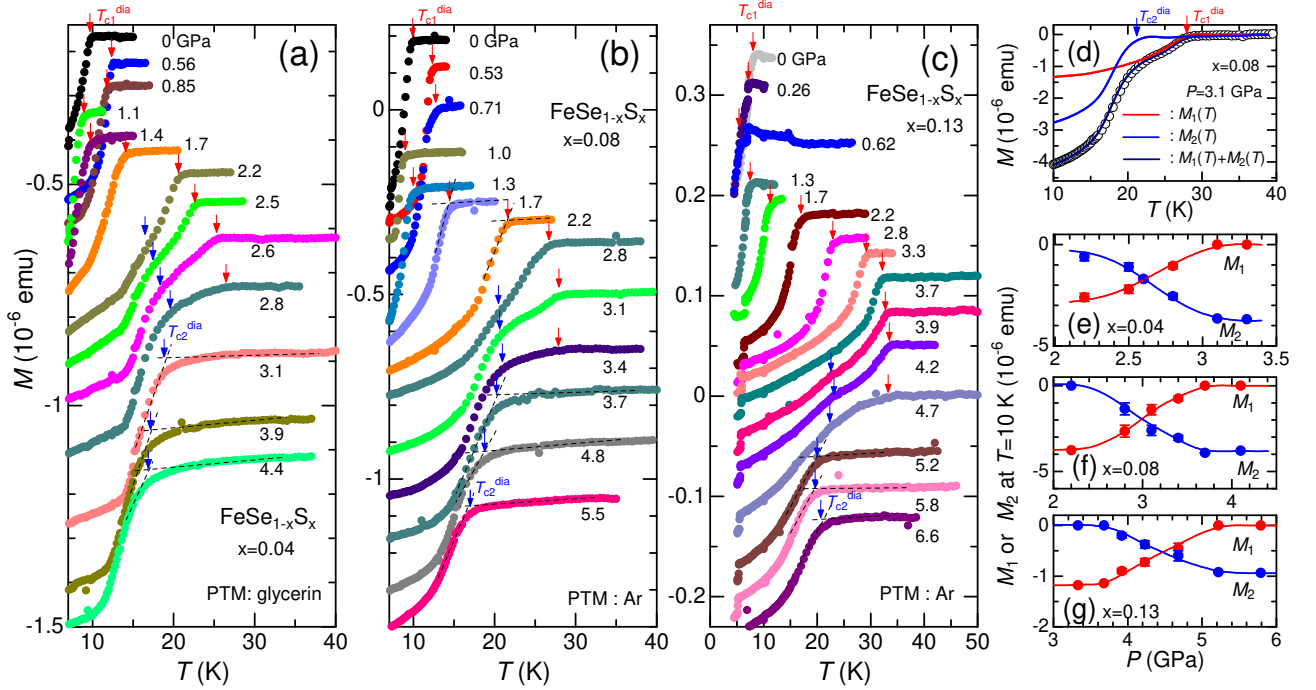


FIG. 1. Temperature (T) dependence of zero-field-cooled dc magnetization (M) measured by applying a magnetic field of 20 Oe for $\text{FeSe}_{1-x}\text{S}_x$ with $x=0.04$ (a), 0.08 (b) and 0.13 (c) at various pressures. The data are intentionally shifted along the longitudinal axis for clarity. A jump in the $M(T)$ curves observed at low temperature for $x=0.13$ is due to SC transition of a Pb manometer. (d) $M(T)$ curve for $x=0.08$ at $P=3.1$ GPa consisting of two components $M_1(T)$ (red solid line) and $M_2(T)$ (blue solid line), each of which shows a diamagnetic behavior below T_{c1}^{dia} and T_{c2}^{dia} , respectively. Plots of amplitude of M_1 and M_2 at $T=10$ K versus pressure for $x=0.04$ (e), 0.08 (f) and 0.13 (g). The solid lines are guide for the eyes.

II. METHODS

Single crystal specimens of $\text{FeSe}_{1-x}\text{S}_x$ ($x=0.04$, 0.08 and 0.13) were obtained by a chemical vapor transport method in a similar way to those described in previous studies[46, 47]. S content x in $\text{FeSe}_{1-x}\text{S}_x$ single crystals used in the measurements were estimated by energy-dispersive X-ray spectroscopy measurements using an analytical scanning electron microscope. Magnetic measurements under high pressure were done by using a miniature diamond anvil cell, which was combined with a sample rod of a commercial SQUID magnetometer. The measurements have been successfully applied to investigate pressure effects on superconductivity in our previous studies[21, 22, 48–50]. The details of the measurements are given in the literature[50]. As the pressure transmitting media (PTM), we used Ar, which is known to be a hydrostatic PTM[51], for the specimens with $x=0.08$ and 0.13 , but glycerine for $x=0.04$, which is hydrostatic below the solidification pressure (~ 5 GPa)[51]. Electrical resistivity measurements under pressure were done by a standard 4-probe technique using an opposed-anvil cell to generate high pressure[52]. For the pressure cell, we used a NiCrAr gasket with a sample hole of $2.2\text{ mm}\phi$, where a $\text{FeSe}_{1-x}\text{S}_x$ single crystal was set together with a high-purity Pb wire for the in-situ determination of pressure from the T_c shift. Also, glycerine was used as PTM

for the measurements.

III. RESULTS AND DISCUSSION

A. dc magnetization

In Figs. 1(a)-1(c), we show zero-field-cooled dc magnetization versus temperature ($M(T)$) data for $x=0.04$, 0.08 and 0.13 measured at various pressures. In Fig. 1(a), the $M(T)$ curve at ambient pressure shows a diamagnetic response below ~ 10 K. The onset temperature of diamagnetic response, which is a reliable marker of T_c and we assign as T_{c1}^{dia} , shifts to a higher temperature at $P=0.56$ GPa but decreases down to ~ 9 K at $P=1.1$ GPa, and then increases again above 1.1 GPa, showing a local maximum at ~ 0.6 GPa. A local maximum below 1 GPa followed by a rapid increase in T_{c1}^{dia} is a characteristic feature seen in FeSe ($x=0$)[22, 50] and also observed for $x=0.08$ in Fig. 1(b). In contrast, as seen in $M(T)$ curves for $x=0.13$ below 1 GPa in Fig. 1(c), T_{c1}^{dia} (~ 8 K at ambient pressure) decreases with increasing pressure but turns to increase above 0.62 GPa, showing no local maximum. The behavior is consistent with that observed for $x=0.12$ in earlier studies[40, 42, 45].

As seen in Figs. 1(a)-1(c), while T_{c1}^{dia} shows a rapid increase above ~ 1 GPa from the minimum value, we should

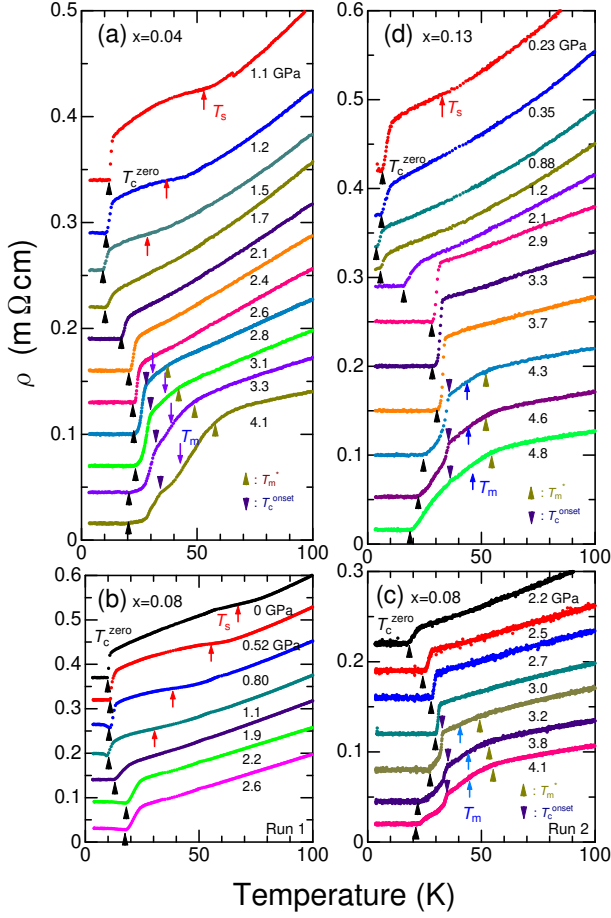


FIG. 2. Temperature dependence of electrical resistivity ρ for $\text{FeSe}_{1-x}\text{S}_x$ with $x=0.04$ (a), 0.08 (run 1) (b), 0.08 (run 2) (c) and 0.13 (d) measured at various pressures using glycerin as the PTM. The data are intentionally shifted along the longitudinal axis for clarity. The black upward triangles indicate zero-resistive temperature T_c^{zero} . The red and blue arrows indicate the nematic (T_s) and magnetic (T_m) transition temperatures, respectively.

note that a hump-like anomaly commonly begins to appear below T_{c1}^{dia} in the $M(T)$ curves at $P=2.2, 2.8$ and 3.9 GPa for $x=0.04, 0.08$ and 0.13 , respectively. In the figures, we assign the hump temperature as T_{c2}^{dia} , since the hump anomaly is thought to correspond to the onset of the second diamagnetic response in the $M(T)$ curves, in other words, the diamagnetic response occurs in two steps. The behavior indicates that there exist two distinct superconducting phases with different T_c s, so that the $M(T)$ curve can be expressed as sum of $M_1(T)$ and $M_2(T)$, each of which exhibit a diamagnetic response below T_{c1}^{dia} and T_{c2}^{dia} , respectively, as shown in Fig. 1(d) for $x=0.08$ at $P=3.1$ GPa as an example. In Figs. 1(a)-1(c), the coexistence of two superconducting phases can be seen in some $M(T)$ curves within a pressure width of ~ 1 GPa, e.g., those at $P=2.8, 3.1$ and 3.4 GPa for $x=0.08$.

We display $M(T)$ curves which are composed of two

diamagnetic components in Figs. S1(a)-S1(i) in Supplemental Material[53], where $M(T)$ curves are expressed as sum of $M_1(T)$ and $M_2(T)$ in a similar manner shown in Fig. 1(d). It should be noted for $x=0.04$ in Figs. S1(a)-S1(d) that $M_1(T)$ which becomes diamagnetic below T_{c1}^{dia} decreases the diamagnetic amplitude with increasing pressure, whereas $M_2(T)$ increases the amplitude with increasing pressure. Similar pressure evolutions of $M_1(T)$ and $M_2(T)$ are also seen for $x=0.08$ and 0.13 . These features are easily confirmed in Fig. 1(e)-1(g), where pressure variations of the amplitude of M_1 and M_2 at $T=10$ K for $x=0.04, 0.08$ and 0.13 are plotted. In the figures, the amplitude of M_1 decreases while that of M_2 increases with increasing pressure, indicating a crossover of superconductivity, i.e., a crossover from the superconductivity described by $M_1(T)$ to $M_2(T)$. Figures 1(e)-1(g) demonstrate continuous transfers in the volume fraction of superconductivity within a pressure width of ~ 1 GPa.

B. Electrical resistivity

In our magnetic measurements, a crossover of the superconductivity was observed under pressure for each specimen. It is important to confirm where the crossover occurs in the phase diagram. Considering the pressure evolution of AFM phase observed in a previous study for $\text{FeSe}_{1-x}\text{S}_x$ with $x=0.04, 0.08$ and 0.12 [29], we notice that the pressure at which the crossover occurs is similar to the pressure above which the AFM phase appears. To confirm whether there is an intimate correlation between the crossover of the superconductivity and the end point of the AFM phase or not and also to construct the phase diagrams, we performed the measurements of $\rho(T)$ under various pressures. The results are shown in Figs. 2(a)-2(d). In the figures, $\rho(T)$ curves show zero-resistivity below T_c^{zero} , indicating a SC transition of $\text{FeSe}_{1-x}\text{S}_x$. Also, the nematic transition is visible as a kink in $\rho(T)$ curves and the transition temperature T_s is determined from the peak of $d\rho/dT$ curve. As examples, we show $\rho(T)$ and $d\rho/dT$ curves at ambient pressure in Figs. S2(a)-S2(c) in Supplemental Material[53]. As seen in Fig. 2(a), the nematic transition for $x=0.04$ is suppressed by the application of pressure and disappears above 1.7 GPa. On the other hand, we note that the transition for $x=0.13$ is suppressed only by the pressure of 0.35 GPa.

In a previous high pressure study using a CAA to generate hydrostatic pressure, transition temperature into the AFM phase T_m was determined by a peak of the $d\rho/dT$ curve in most cases[29]. The peak was observed between the onset temperature of resistive drop associated with superconductivity T_c^{onset} and T_m^* below which $\rho(T)$ begins to decrease due to the evolution of AFM correlation which reduces the magnetic scattering. However, we failed to observe a clear peak of $d\rho/dT$ between T_c^{onset} and T_m^* in the present work, probably due to the difference in the degree of pressure homogeneity. Thus,

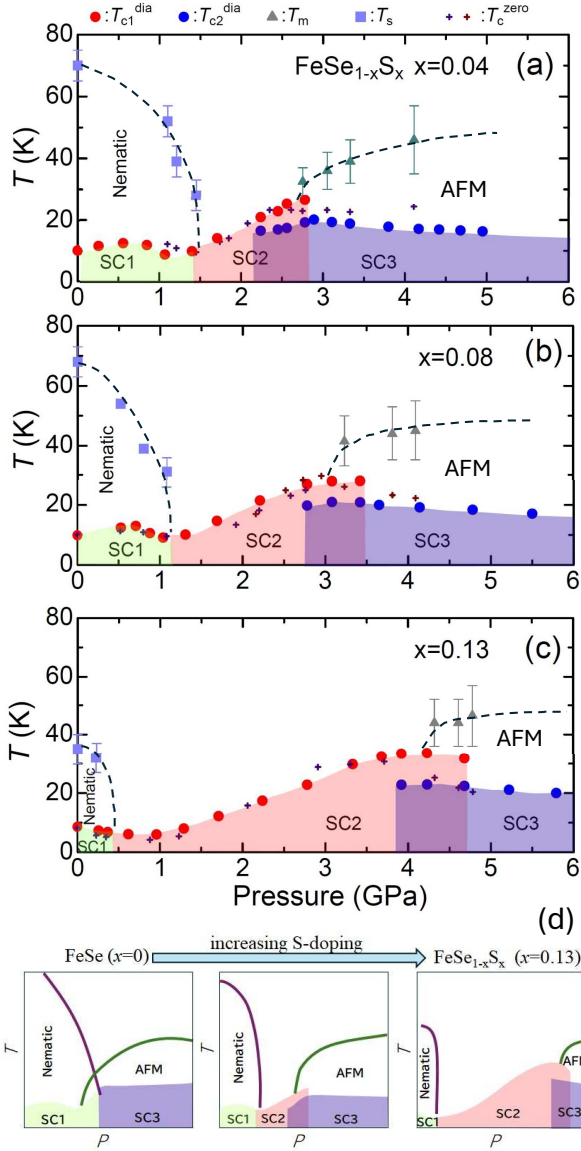


FIG. 3. T - P phase diagram of $\text{FeSe}_{1-x}\text{S}_x$ with $x=0.04$ (a), 0.08 (b) and 0.13 (c). The broken lines are guide for the eyes. (d) Schematic view of the variation of the T - P phase diagram of $\text{FeSe}_{1-x}\text{S}_x$ with increasing x .

we define a midpoint of T_m^* and T_c^{onset} as T_m in Figs. 2(a)-2(d).

C. T - P phase diagram

Figures 3(a)-3(c) display T - P phase diagrams of $\text{FeSe}_{1-x}\text{S}_x$, where the phase boundaries of SC phases are described by T_{c1}^{dia} and T_{c2}^{dia} obtained by the dc magnetization measurements. In the figures, it is found that the nematic phase shrinks with increasing x . The behavior agrees with that reported in an early work[45]. Moreover, the AFM phase moves to the higher pressure region with increasing x , so that the S-substitution extends the

region where the SC phase exists alone in the intermediate pressure range without coexisting nematic or AFM phases. The evolution of AFM phase with increasing x in the T - P phase diagram and the pressures above which the AFM phase appear are consistent with that observed by the measurements using a CAA[29]. We denote the SC phases below and above the nematic end point as SC1 and SC2, respectively, since two distinct superconductivities are expected to be realized due to the reconstitution of Fermi surfaces across the nematic end point[40–44]. It is also found that two SC phases with different T_c s overlap within a pressure width of $\Delta P \sim 1$ GPa, showing a crossover of the superconductivity. We also denote the SC phase realized after the crossover from SC2 as SC3. It should be noted that the occurrence of crossover from SC2 to SC3 across the end point of AFM phase is confirmed in the phase diagrams, demonstrating that the mechanism of the superconductivity is different inside and outside the AFM phase. Although zero-resistivity is a good marker of SC transition, T_c^{zero} is found to be between T_{c1}^{dia} and T_{c2}^{dia} in the crossover pressure region. We could not observe a successive SC transition by $\rho(T)$ measurements, since nothing could be reflected on $\rho(T)$ when $\rho(T)$ becomes zero below the first T_c .

D. Discussion

In Fig. 3(d), a schematic view of the evolution of the T - P phase diagram with x is shown. SC2 phase is an intermediate phase between SC1 and SC3 phases, which coexist with the nematic or AFM phases. Thus, for $x=0$, the intermediate SC2 phase would not exist, since the nematic and AFM phases are too close and overlap to each other, while high- T_c SC phase is known to appear above the pressure where the AFM phase terminates. One may consider that high- T_c superconductivity of SC2 phase is realized to be enhanced by AFM and/or nematic fluctuations, since SC2 phase locates between the nematic and magnetic phases. If this is the case, a gap of T_c between SC2 and SC3 phases are attributable to a reduction of AFM fluctuations inside the AFM phase. We can see that the T_c gap becomes remarkable for $x=0.13$ in Fig. 3(c). This could be viewed as evidence that the AFM fluctuations become dominant to enhance the superconductivity due to the shrink of the nematic phase for $x=0.13$. Nevertheless, the effect of AFM fluctuations may be uncertain, since AFM fluctuations are expected to be relatively weak, considering the fact that the transition at T_m is first-order type due to a spin-lattice coupling[25, 26], as also reported that the low- T_c SC1 dome below 1 GPa is accompanied by strong AFM fluctuations, whereas high- T_c SC2 dome develops above 1 GPa with fairly weak AFM fluctuations[40, 42].

On the other hand, the effect of nematic fluctuations for the SC2 phase above the nematic end point is also unclear, since nematic fluctuations are thought to be quenched at the nematic end point probably due

to the strong coupling to the lattice or local strain effects[43]. Interestingly, also for pristine FeSe, the collapse of nematic fluctuations above 1 GPa has been reported and it plays a marginal role for the high- T_c superconductivity[28], stressing the difference from other iron-based superconductors, where both nematic and magnetic phases closely coexist and superconductivity is enhanced at the critical point. Recent microscopic measurements on the evolution of precise gap structure with increasing x across the nematic critical point x_c in $\text{FeSe}_{1-x}\text{S}_x$ have revealed the superconductivity for $x > x_c$ is mediated by nematic fluctuations[39]. To clarify the origin of SC2 and SC3, microscopic measurements under pressure which unveil the gap structure and Fermi surface reconstitution across the end point of AFM phase are essential as well. Occurrence of a Fermi surface reconstruction in the crossover region is likely in $\text{FeSe}_{1-x}\text{S}_x$, as it was inferred from a sudden change in the Shubnikov-de Haas oscillation with the emergence of AFM phase in FeSe[54].

IV. SUMMARY

We have investigated T - P phase diagram of $\text{FeSe}_{1-x}\text{S}_x$ by the measurements of dc magnetization and electrical resistivity under pressure. It was found that $M(T)$ curves near the pressure where the AFM emerges show a diamagnetic response in two steps, indicating a coexistence of two distinct SC phases with different T_c s. The characteristic behavior was observed for a pressure width of ~ 1 GPa, where continuous transfer in the volume fraction of SC phases was indicated from the pressure variation of diamagnetic amplitude, suggesting a crossover of the superconductivity together with the emergence of AFM phase. Microscopic measurements which reveal the SC gap structure and the evolution of Fermi surface under pressure inside and outside the AFM phase are highly desired to elucidate the mechanism of superconductivities.

ACKNOWLEDGMENTS

The authors thank Shijo Nisigori, Takahiro Matsumoto, Kazuya Ando, Ryuichi Miyake, Kai Miyamoto for technical assistance.

-
- [1] Y. Kamihara, T. Watanabe, M. Hirano, and H. Hosono, J. Am. Chem. Soc. **130**, 3296 (2008).
 - [2] H. Hosono, and K. Kuroki, Physica C **514**, 399 (2015).
 - [3] T. Shibauchi, T. Hanaguri, Y. Matsuda, J. Phys. Soc. Jpn. **89**, 102002 (2020).
 - [4] R. M. Fernandes, A. I. Coldea, H. Ding, i. R. Fisher, P. J. Hirschfeld and G. Kotliar, Nature **601**, 35 (2022).
 - [5] M. Rotter, M. Tegel and D. Johrendt, Phys. Rev. Lett. **101**, 107006 (2008).
 - [6] S. Kasahara, H. J. Shi, K. Hashimoto, S. Tonegawa, Y. Mizukami, T. Shibauchi, K. Sugimoto, T. Fukuda, T. Terashima, A. H. Nevidomskyy and Y. Matsuda, Nature **486**, 382 (2012).
 - [7] M. S. Torikachvili, S. L. Bud'ko, N. Ni, and P. C. Canfield, Phys. Rev. B **78**, 104527 (2008).
 - [8] E. Colombier, S. L. Bud'ko, N. Ni, and P. C. Canfield, Phys. Rev. B **79**, 224518 (2009).
 - [9] K. Matsubayashi, N. Katayama, K. Ohgushi, A. Yamada, K. Munakata, T. Matsumoto, and Y. Uwatoko, J. Phys. Soc. Jpn. **78**, 073706 (2009).
 - [10] T. Terashima, M. Kimata, H. Satsukawa, A. Harada, K. Hazama, S. Uji, H. S. Suzuki, T. Matsumoto, and K. Murata, J. Phys. Soc. Jpn. **78**, 083701 (2009).
 - [11] H. Luetkens, H.-H. Klauss, M. Kraken, F. J. Litterst, T. Dellmann, R. Klingeler, C. Hess, R. Khasanov, A. Amato, C. Baines, M. Kosmala, O. J. Schumann, M. Braden, J. Hamann-Borrero, N. Leps, A. Kondrat, G. Behr, J. Werner, and B. Büchner, Nat. Mater. **8**, 305 (2009).
 - [12] D. R. Parker, M. J. P. Smith, T. Lancaster, A. J. Steele, I. Franke, P. J. Baker, F. L. Pratt, M. J. Pitcher, S. J. Blundell, and S. J. Clarke, Phys. Rev. Lett. **104**, 057007 (2010).
 - [13] A. F. Wang, X. G. Luo, Y. J. Yan, J. J. Ying, Z. J. Xiang, G. J. Ye, P. Cheng, Z. Y. Li, W. J. Hu, and X. H. Chen, Phys. Rev. B **85**, 224521 (2012).
 - [14] A. F. Wang, J. J. Lin, P. Cheng, G. J. Ye, F. Chen, J. Q. Ma, X. F. Lu, B. Lei, X. G. Luo, and X. H. Chen, Phys. Rev. B **88**, 094516 (2013).
 - [15] K. Ueshima, F. Han, X. Zhu, H. H. Wen, S. Kawasaki, and G. -q. Zheng, Phys. Rev. B **89**, 184506 (2014).
 - [16] S. Hohenstein, F. Hummel, Z. Guguchia, S. Kamusell, N. Barbero, H. Ogino, Z. Shermadini, R. Khasanov, A. Amato, T. Shiroka, H.-H. Klauss, E. Morenzoni, D. Johrendt, and H. Luetkens, arXiv:1911.04319.
 - [17] S. Masaki, H. Kotegawa, Y. Hara, H. Tou, K. Murata, Y. Mizuguchi, and Y. Takano, J. Phys. Soc. Jpn. **78**, 063704 (2009).
 - [18] S. Medvedev, T. M. McQueen, I. A. Troyan, T. Palasyuk, M. I. Erements, R. J. Cava, S. Naghavi, F. Casper, V. Ksenofontov, G. Wortmann, and C. Felser, Nat. Mater. **8**, 630 (2009).
 - [19] S. Margadonna, Y. Takabayashi, Y. Ohishi, Y. Mizuguchi, Y. Takano, T. Kagayama, T. Nakagawa, M. Takata, and K. Prassides, Phys. Rev. B **80**, 064506 (2009).
 - [20] D. Braithwaite, B. Salce, G. Lapertot, F. Bourdarot, C. Marin, D. Aoki, and M. Hanfland, J. Phys.: Condens. Matter **21**, 232202 (2009).
 - [21] K. Miyoshi, Y. Takaichi, E. Mutou, K. Fujiwara, and J. Takeuchi, J. Phys. Soc. Jpn. **78**, 093703 (2009).
 - [22] K. Miyoshi, K. Morishita, E. Mutou, M. Kondo, O. Seida, K. Fujiwara, J. Takeuchi, and S. Nishigori, J. Phys. Soc. Jpn. **83**, 013702 (2014).
 - [23] T. Terashima, N. Kikugawa, S. Kasahara, T. Watashige, T. Shibauchi, Y. Matsuda, T. Wolf, A. E. Böhmer, F.

- Hardy, C. Meingast, H. v. Löhneysen, and S. Uji, *J. Phys. Soc. Jpn.* **84**, 063701 (2015).
- [24] J. P. Sun, K. Matsuura, G. Z. Ye, Y. Mizukami, M. Shimozaawa, K. Matsubayashi, M. Yamashita, T. Watashige, S. Kasahara, Y. Matsuda, J. -Q. Yan, B. C. Sales, Y. Uwatoko, J. -G. Cheng and T. Shibauchi, *Nat. Commun.* **7**, 12146 (2016).
- [25] P. S. Wang, S. S. Sun, Y. Cui, W. H. Song, T. R. Li, R. Yu, H. Lei, and W. Yu, *Phys. Rev. Lett.* **117**, 237001 (2016).
- [26] K. Kothapalli, A. E. Böhrer, W. T. Jayasekara, B. G. Ueland, P. Das, A. Sapkota, V. Taufour, Y. Xiao, E. Alp, S. L. Bud'ko, P. C. Canfield, A. Kreyssig, and A. I. Goldman, *Nat. Commun.* **7**, 12728 (2016).
- [27] R. Khasanov, Z. Guguchia, A. Amato, E. Morenzoni, X. Dong, F. Zhou, and Z. Zhao *Phys. Rev. B* **95**, 180504(R) (2017).
- [28] P. Massat, Y. Quan, R. Grasset, M. Measson, M. Caza-yous, A. Sacuto, S. Karlsson, P. Strobel, P. Toulemonde, Z. Yin and Y. Gallais, *Phys. Rev. Lett.* **121**, 077001 (2018).
- [29] K. Matsuura, Y. Mizukami, Y. Arai, Y. Sugimura, N. Maejima, A. Machida, T. Watanuki, T. Fukuda, T. Yajima, Z. Hiroi, K. Y. Yip, Y.C. Chan, Q. Niu, S. Hosoi, K. Ishida, K. Mukasa, S. Kasahara, J.-G. Cheng, S.K. Goh, Y. Matsuda, Y. Uwatoko and T. Shibauchi, *Nat. Commun.* **8**, 1143 (2017).
- [30] S. Licciardello, J. Buhot, J. Lu, J. Ayres, S. Kasahara, Y. Matsuda, T. Shibauchi, and N. E. Hussey, *Nature* **567**, 213 (2019).
- [31] K. Ishida, Y. Onishia, M. Tsujii, K. Mukasa, M. Qiu, M. Saito, Y. Sugimura, K. Matsuura, Y. Mizukami, K. Hashimoto and T. Shibauchi, *Proc. Natl. Acad. Sci. USA* **119**, e2110501119 (2022).
- [32] P. Wiecki, K. Rana, A. E. Bohmer, Y. Lee, S. L. Bud'ko, P. C. Canfield and Y. Furukawa, *Phys. Rev. B* **98**, 020507(R) (2018).
- [33] J. Kang, R. M. Fernandes and A. Chubukov, *Phys. Rev. Lett.* **120**, 267001 (2018).
- [34] P. O. Sprau, A. Kostin, A. Kreisel, A. E. Bohmer, V. Taufour, P. C. Canfield, S. Mukherjee, P. J. Hirschfeld, B. M. Andersen, J. C. Seamus Davis, *Science* **357**, 75 (2017).
- [35] L. Benfatto, B. Valenzuela and L. Fanfarillo *npj Quantum Mater.* **3**, 56 (2018).
- [36] Y. Sato, S. Kasahara, T. Taniguchia, X. Xing, Y. Kasahara, Y. Tokiwab, Y. Yamakawa, H. Kontani, T. Shibauchi, and Y. Matsuda, *Proc. Natl. Acad. Sci. USA* **115**, 1227 (2018).
- [37] T. Hanaguri, K. Iwaya, Y. Kohsaka, T. Machida, T. Watashige, S. Kasahara, T. Shibauchi, Y. Matsuda, *Sci. Adv.* **4**, eaar6419 (2018).
- [38] A. I. Coldea, S. F. Blake, S. Kasahara, A. A. Haghighirad, M. D. Watson, W. Knafo, E. -S. Choi, A. McCollam, P. Reiss, T. Yamashita, M. Bruma, S. C. Speller, Y. Matsuda, T. Wolf, T. Shibauchi and A. J. Schofield, *npj Quantum Mater.* **4**, 2 (2019).
- [39] P. K. Nag, K. Scott, V. S. de Carvalho, J. K. Byland, X. Yang, M. Walker, A. G. Greenberg, P. Klavins, E. Miranda, A. Gozar, V. Taufour, R. M. Fernandes and E. H. da Silva Neto, *Nat. Phys.* **21**, 89 (2025).
- [40] T. Kuwayama, K. Matsuura, Y. Mizukami, S. Kasahara, Y. Matsuda, T. Shibauchi, Y. Uwatoko and N. Fujiwara, *J. Phys. Soc. Jpn.* **88**, 033703 (2019).
- [41] K. Rana, L. Xiang, P. Wiecki, R. A. Ribeiro, G. G. Lesseux, A. E. Böhrer, S. L. Bud'ko, P. C. Canfield, and Y. Furukawa, *Phys. Rev. B* **101**, 180503 (2020).
- [42] T. Kuwayama, K. Matsuura, J. Gouchi, Y. Yamakawa, Y. Mizukami, S. Kasahara, Y. Matsuda, T. Shibauchi, H. Kontani, Y. Uwatoko and N. Fujiwara, *Sci. Rep.* **11**, 17265 (2021).
- [43] P. Reiss, D. Graf, A. Haghighirad, W. Knafo, L. Drigo, M. Bristow, A. J. Schofield and A. I. Coldea, *Nat. Phys.* **16**, 89 (2020).
- [44] Y. Yamakawa and H. Kontani, *Phys. Rev. B* **96**, 144509 (2017).
- [45] Li Xiang, U. S. Kaluarachchi, A. E. Böhrer, V. Taufour, M. A. Tanatar, R. Prozorov, S. L. Bud'ko and P. C. Canfield, *Phys. Rev. B* **96**, 024511 (2017).
- [46] K. Miyoshi, A. Shiot, S. Kato, S. Yamamoto, K. Fujiwara and S. Nishigori, *JPS Conf. Proc.* **30**, 011068 (2020).
- [47] K. Miyoshi, D. Izuhara, Y. Yamamoto, *JPS Conf. Proc.* **38**, 011024 (2023).
- [48] K. Miyoshi, Y. Takaichi, Y. Takamatsu, M. Miura, and J. Takeuchi, *J. Phys. Soc. Jpn.* **77**, 043704 (2008).
- [49] K. Miyoshi, E. Kojima, S. Ogawa, Y. Shimojo, and J. Takeuchi, *Phys. Rev. B* **87**, 235111 (2013).
- [50] K. Miyoshi, S. Yamamoto, A. Shiot, T. Matsuoka, M. Ohe, Y. Yamamoto and S. Nishigori, *J. Phys. Soc. Jpn.* **90**, 073706 (2021).
- [51] N. Tateiwa and Y. Haga, *Rev. Sci. Instrum.* **80**, 123901 (2009).
- [52] K. Kitagawa, H. Gotou, T. Yagi, A. Yamada, T. Matsumoto, Y. Uwatoko, and M. Takigawa, *J. Phys. Soc. Jpn.* **79**, 024001 (2010).
- [53] See Supplemental Material at [URLwillbeinsertedby-publisher](#) for additional figures.
- [54] T. Terashima, N. Kikugawa, A. Kiswandhi, D. Graf, E. -S. Choi, J. Brooks, S. Kasahara, T. Watashige, Y. Matsuda, T. Shibauchi, T. Wolf, A. E. Böhrer, F. Hardy, C. Meingast, H. v. Löhneysen, and S. Uji, *Phys. Rev. B* **93**, 094505 (2016).